

## Article

# UV Stimulated Manganese Dioxide for the Persulfate Catalytic Degradation of Bisphenol A

Guihua Dong<sup>1</sup>, Bing Chen<sup>1,\*</sup> , Bo Liu<sup>1</sup>, Stanislav R. Stoyanov<sup>2,\*</sup>, Yiqi Cao<sup>1</sup>, Min Yang<sup>1</sup> and Baiyu Zhang<sup>1</sup> 

<sup>1</sup> Northern Region Persistent Organic Pollution Control (NRPOP) Laboratory, Faculty of Engineering and Applied Science, Memorial University of Newfoundland, St. John's, NL A1B 3X5, Canada; gdong@mun.ca (G.D.); bl4184@mun.ca (B.L.); yiqic@mun.ca (Y.C.); min.yang@mun.ca (M.Y.); bzhang@mun.ca (B.Z.)

<sup>2</sup> Natural Resources Canada, CanmetENERGY Devon, 1 Oil Patch Drive, Devon, AB T9G 1A8, Canada

\* Correspondence: bchen@mun.ca (B.C.); stanislav.stoyanov@canada.ca (S.R.S.)

**Abstract:** One of the most commonly produced industrial chemicals worldwide, bisphenol A (BPA), is used as a precursor in plastics, resins, paints, and many other materials. It has been proved that BPA can cause long-term adverse effects on ecosystems and human health due to its toxicity as an endocrine disruptor. In this study, we developed an integrated MnO<sub>2</sub>/UV/persulfate (PS) process for use in BPA photocatalytic degradation from water and examined the reaction mechanisms, degradation pathways, and toxicity reduction. Comparative tests using MnO<sub>2</sub>, PS, UV, UV/MnO<sub>2</sub>, MnO<sub>2</sub>/PS, and UV/PS processes were conducted under the same conditions to investigate the mechanism of BPA catalytic degradation by the proposed MnO<sub>2</sub>/UV/PS process. The best performance was observed in the MnO<sub>2</sub>/UV/PS process in which BPA was completely removed in 30 min with a reduction rate of over 90% for total organic carbon after 2 h. This process also showed a stable removal efficiency with a large variation of pH levels (3.6 to 10.0). Kinetic analysis suggested that <sup>1</sup>O<sub>2</sub> and SO<sub>4</sub><sup>•−</sup> played more critical roles than •OH for BPA degradation. Infrared spectra showed that UV irradiation could stimulate the generation of –OH groups on the MnO<sub>2</sub> photocatalyst surface, facilitating the PS catalytic degradation of BPA in this process. The degradation pathways were further proposed in five steps, and thirteen intermediates were identified by gas chromatography-mass spectrometry. The acute toxicity was analyzed during the treatment, showing a slight increase (by 3.3%) in the first 30 min and then a decrease by four-fold over 2 h. These findings help elucidate the mechanism and pathways of BPA degradation and provide an effective PS catalytic strategy.

**Keywords:** BPA; UV stimulated MnO<sub>2</sub>; photocatalytic degradation; synergistic effect; pathways; toxicity



**Citation:** Dong, G.; Chen, B.; Liu, B.; Stoyanov, S.R.; Cao, Y.; Yang, M.; Zhang, B. UV Stimulated Manganese Dioxide for the Persulfate Catalytic Degradation of Bisphenol A. *Catalysts* **2021**, *11*, 502. <https://doi.org/10.3390/catal11040502>

Academic Editors: Cassan Hodaifa and Rafael Borja

Received: 24 March 2021

Accepted: 14 April 2021

Published: 16 April 2021

**Publisher's Note:** MDPI stays neutral with regard to jurisdictional claims in published maps and institutional affiliations.



**Copyright:** © 2021 by the authors. Licensee MDPI, Basel, Switzerland. This article is an open access article distributed under the terms and conditions of the Creative Commons Attribution (CC BY) license (<https://creativecommons.org/licenses/by/4.0/>).

## 1. Introduction

Bisphenol A (BPA) is a high-production-volume industrial chemical used as a precursor in synthetic polycarbonate plastics and epoxy resins, as well as many consumer products, including food containers, paper products, toys, medical equipment, and electronics [1]. Growing evidence has shown the long-term negative effects of BPA on aquatic life and human health [2,3]. Several studies have reported on the potential adverse effects of BPA exposure to humans during critical stages of neonatal or early development [3,4]. Meanwhile, BPA was ubiquitously detected in river water and soil at microgram levels [5,6]. Moreover, the highest BPA concentrations were found in landfill leachate in Japan (up to 17.2 mg/L) and Germany (4.2–25 mg/L) [7–9]. Growing concerns have been raised on the associated environmental risks caused by BPA as both a sole emerging contaminant and co-contaminant [10–12], leading to urgent demands for effective remediation techniques towards contaminated waters.

Advanced oxidation processes (AOPs) based on the production of hydroxyl radical (•OH), which acts as a powerful oxidant, have been regarded as highly promising for the

degradation of BPA [13,14]. Persulfate-based AOPs have drawn considerable attention in recent years due to their high efficiency for generating sulfate radical ( $\text{SO}_4^{\bullet-}$ ), which has more positive redox potential (2.6–3.1 V) than  $\bullet\text{OH}$  (1.9–2.7 V), to degrade recalcitrant organic pollutants [15,16]. Persulfate (PS) is one of the main precursors for the generation of  $\text{SO}_4^{\bullet-}$  [17,18]. PS can be activated by transition metal catalysts (such as iron oxides and manganese oxides), nonmetal catalysts, ultraviolet (UV) and visible light, ultrasound, alkaline, heat, and strong oxidants to produce  $\text{SO}_4^{\bullet-}$  and other radicals for the removal of organic pollutants [19,20].

Synergistic PS catalytic activation was recently demonstrated with enhanced contaminants removal. Most attention has been paid to the applications of transition metals or their oxides (e.g., iron, copper, and cobalt) and UV as hybrid activators for PS catalytic activation [21–23]. In fact, manganese dioxide ( $\text{MnO}_2$ ) is widely used as a catalyst or activator in various heterogeneous reaction systems due to its high natural abundance, low toxicity, and low environmental impacts [24–26].  $\text{MnO}_2$  is a promising candidate for photocatalyst application due to its narrow bandgap (1–2 eV) and ability to absorb light under solar energy [27]. However, to our best knowledge, synergistic use of  $\text{MnO}_2$  and UV has never been applied for PS activation. Recently, Eslami et al. [28] confirmed that the synergistic use of  $\text{MnO}_2$  and UV is a promising hybrid activator for peroxymonosulfate (PMS) activation. Accordingly, there are many distinctive differences during activation of PS and PMS, especially in reactivity toward radicals and responses to different pH levels [29]. Furthermore, the synergistic mechanism for PS catalytic activation, especially the interactions between  $\text{MnO}_2$  and UV, remains unknown and deserves further investigation.

In this study, we first developed an enhanced  $\text{MnO}_2/\text{UV}/\text{PS}$  process for the efficient removal and mineralization of BPA. The optimum activation performance of UV irradiation and  $\text{MnO}_2$  in various conditions was examined in detail. The enhanced BPA degradation mechanism in the hybrid catalytic process was then explored using quenching studies for reactive oxygen species (ROS). More importantly, the effect of UV irradiation on the  $\text{MnO}_2$  surface in this process was substantially investigated. Moreover, the complex BPA degradation mechanism was presented in terms of the predominant reaction pathways, supported by intermediates identified using gas chromatography-mass spectrometry (GC-MS). Finally, the acute toxicity due to the BPA removal through the  $\text{MnO}_2/\text{UV}/\text{PS}$  process was evaluated.

## 2. Results and Discussion

### 2.1. Degradation and Mineralization of BPA

To evaluate and compare the BPA degradation and mineralization performance of the  $\text{MnO}_2/\text{UV}/\text{PS}$  process with those of its component processes, seven different processes (namely PS,  $\text{MnO}_2$ , UV, UV/ $\text{MnO}_2$ ,  $\text{MnO}_2/\text{PS}$ , UV/PS, and  $\text{MnO}_2/\text{UV}/\text{PS}$ ) were tested (Figure 1).

The PS process alone had no effect on BPA removal, while only 3.6% of BPA could be removed by the  $\text{MnO}_2$  process after 2 h (Figure 1a). Lin et al. [30] reported the relatively high efficacy of BPA removal from a 4.4  $\mu\text{M}$  solution using a high concentration of 800  $\mu\text{M}$   $\text{MnO}_2$  over 10 min. The low BPA removal efficiency of our  $\text{MnO}_2$  process might be due to its relatively low concentration of  $\text{MnO}_2$  compared to BPA. The individual applications of  $\text{MnO}_2$  and PS were ineffective, presumably due to slow (or no) free radical generation and negligible absorption capacity of  $\text{MnO}_2$  in this study. Both UV and UV/ $\text{MnO}_2$  processes degraded 75.0% and 85.0% of BPA in 2 h, respectively. In the  $\text{MnO}_2/\text{PS}$  process, the removal efficiency of 87.8% was observed after 2 h, whereas the UV-activated PS process could effectively remove all BPA in 45 min. The synergistic PS catalytic activation by  $\text{MnO}_2/\text{UV}$  could entirely remove BPA within 30 min. Both the UV/PS and  $\text{MnO}_2/\text{UV}/\text{PS}$  processes had better performances than the  $\text{MnO}_2/\text{PS}$  process, and the concurrent presence of UV and  $\text{MnO}_2$  further enhanced the PS catalytic activation, and consequently, the BPA degradation.

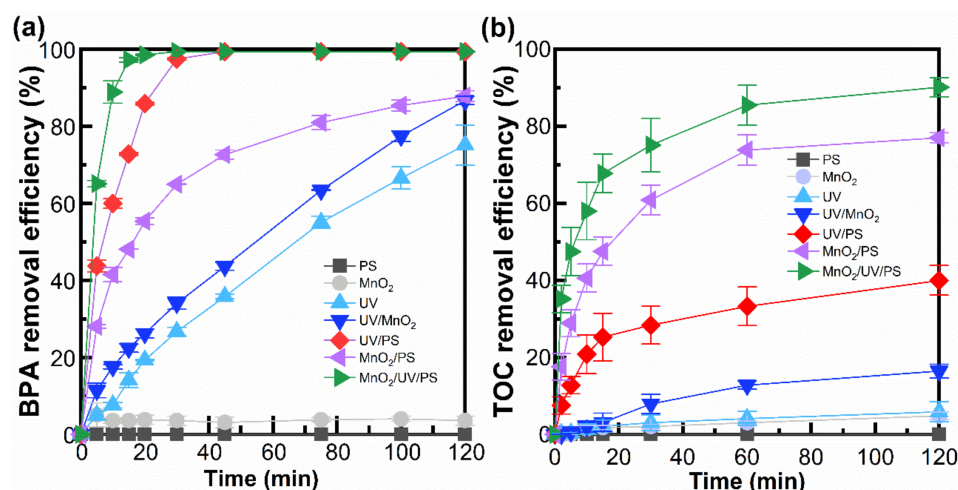


**Figure 1.** BPA (a) and TOC (b) removal over time using the PS, MnO<sub>2</sub>, UV, UV/MnO<sub>2</sub>, MnO<sub>2</sub>/PS, UV/PS, and MnO<sub>2</sub>/UV/PS processes. Conditions at t = 0 min: [BPA] = 30 mg/L, [PS] = 1 mM, [MnO<sub>2</sub>] = 0.25 g/L, pH = 6.5, T = 22–25 °C.

A TOC analyzer was employed to explore the mineralization of BPA in the above-noted seven processes. Figure 1b shows that the TOC removal efficiencies of these seven processes were quite different. The TOC removal efficiencies of the PS, MnO<sub>2</sub>, and UV processes after 2 h of treatment were 0%, 4.8%, and 5.8%, respectively, indicating the sole processes could barely mineralize BPA from the aqueous phase. The TOC removal efficiency in the UV/MnO<sub>2</sub> process was enhanced to 16.4%, which implied the combination of UV irradiation and MnO<sub>2</sub> had a positive effect on BPA mineralization. The MnO<sub>2</sub>/PS process further increased the removal efficiency to 77.0%. Huang and Zhang [31] suggested that MnO<sub>2</sub> activated PS could promote the generation of radicals (such as SO<sub>4</sub><sup>•−</sup> and •OH) to remove organic pollutants. The results of the UV/PS process showed that BPA could be removed entirely in 45 min, but the TOC value remained high, even after 2 h of treatment (40.0% of the mineralization rate). PS residuals in the MnO<sub>2</sub>/PS, UV/PS, and MnO<sub>2</sub>/UV/PS processes (Figure S1) suggested the UV irradiation was the main factor in the acceleration of PS decomposition. Meanwhile, the MnO<sub>2</sub>/PS process showed high effectiveness in the BPA mineralization. Remarkably, the MnO<sub>2</sub>/UV/PS process could achieve more than 90.0% of TOC removal efficiency in 2 h, which demonstrated that PS activation by the combination of UV and MnO<sub>2</sub> could effectively improve the BPA and TOC removal from water.

## 2.2. Effects of MnO<sub>2</sub> Dosages, PS Concentrations, and pH Levels on BPA Degradation

We further evaluated the effects of the MnO<sub>2</sub> dosages, PS concentrations, and pH levels on BPA degradation using the MnO<sub>2</sub>/UV/PS process within 30 min. Figure 2a shows that the extent of BPA degradation was gradually promoted with the increased MnO<sub>2</sub> dosages (0.05–0.30 g/L) due to the availability of more surface sites for PS activation. Complete BPA degradation was observed with a MnO<sub>2</sub> dosage of 0.25 g/L; further increasing dosages slightly improved degradation. The effects of PS concentrations were then evaluated under the conditions of 0.25 g/L MnO<sub>2</sub> and UV irradiation (Figure 2b). Compared with the effect of MnO<sub>2</sub>, increasing PS concentration enhanced BPA degradation to a greater extent, leading to a complete BPA removal at 1 mM PS. The further increase of PS dosages only promoted the removal rate slightly, indicating that the concentration of 1 mM was sufficient for BPA degradation. Therefore, 0.25 g/L MnO<sub>2</sub> and 1 mM PS was optimized for the efficient degradation of BPA in our study.

As can be seen, BPA could be effectively degraded with an efficiency of over 80% in a wide range of pH levels (3.6 to 10.0) (Figure 2c). The degradation rate was relatively low under acidic conditions (pH 3.6 and 5.0). The lowest reaction rate occurred at pH 5.0. According to the reports by Criquet and Leitner [32], this phenomenon was caused by

the increased consumption of  $\text{SO}_4^{\bullet-}$  by acetic acid in buffer at pH 5.0 compared to other pH levels. At pH 6.5, the improved BPA degradation was achieved comparing with acidic conditions. At pH 8.0 and 10.0, a slight improvement of BPA degradation could be due to the additional PS activation by alkaline conditions [33]. Lee, Von Gunten, and Kim [29] suggested that the main oxidants may change from  $\text{SO}_4^{\bullet-}$  to  $\bullet\text{OH}$  under alkaline conditions, leading to the abatement of organics that persisted in PS activation. From Figure 2d, the PS decomposition rate can be seen to have gradually increased along with the increased pH value. In contrast, the contaminant degradation was significant in acidic (pH 4.0) conditions, and decreased at neutral (pH 7.0) and alkaline (pH 10.0) conditions in the PMS activation process [28]. The high efficiency of the  $\text{MnO}_2/\text{UV}/\text{PS}$  oxidation process in a wide range of pH levels (pH from 3.6 to 10.0) suggests its robust capacity in treating wastewater with broad pH ranges.

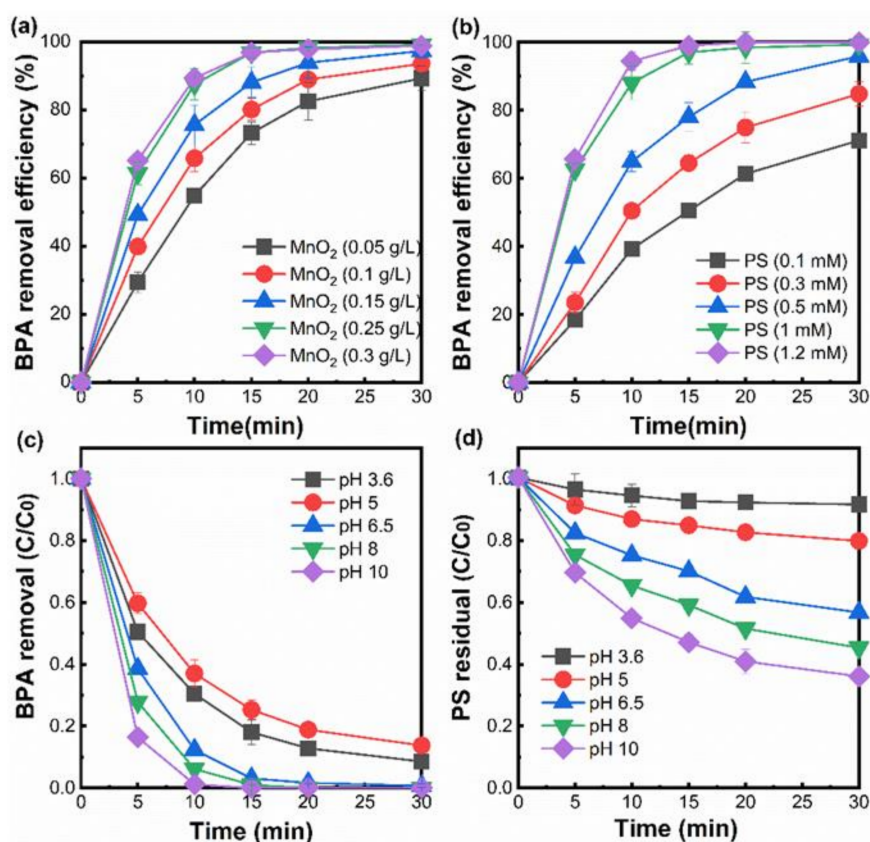


**Figure 2.** Effects of (a)  $\text{MnO}_2$  dosages, (b) PS concentration, and (c) pH level on BPA removal, and PS residual in different pH levels (d). Conditions at  $t = 0$  min:  $[\text{BPA}] = 30$  mg/L, pH in (a) and (b) = 6.5,  $[\text{PS}]$  in (a) and (c) = 1 mM,  $[\text{MnO}_2]$  in (b) and (c) = 0.25 g/L.

### 2.3. Kinetic Evaluation and Reaction Mechanism Analysis

#### 2.3.1. Synergistic Effect of $\text{MnO}_2$ and UV

Batch tests of three processes ( $\text{MnO}_2/\text{PS}$ ,  $\text{UV}/\text{PS}$ , and  $\text{MnO}_2/\text{UV}/\text{PS}$ ) were implemented for 30 min to explore the synergistic effect of  $\text{MnO}_2$  and UV as the hybrid catalyst of PS. The pseudo-first-order kinetic behaviors of the three processes are shown in Figure 3. The rate constants of both the  $\text{MnO}_2/\text{PS}$  process ( $k_{\text{MnO}_2/\text{PS}} = 0.0334 \text{ min}^{-1}$ ) and the  $\text{UV}/\text{PS}$  process ( $k_{\text{UV}/\text{PS}} = 0.1177 \text{ min}^{-1}$ ) were found to be lower than that of the  $\text{MnO}_2/\text{UV}/\text{PS}$  process ( $k_{\text{MnO}_2/\text{UV}/\text{PS}} = 0.2196 \text{ min}^{-1}$ ). The degree of synergy between  $\text{MnO}_2$  and UV as the hybrid catalyst was calculated from the rate constants according to Equation (1) [34]. The calculated degree of synergy value (%S) of 31.2% for the hybrid  $\text{MnO}_2/\text{UV}/\text{PS}$  process reflected the synergistic PS catalytic activation by  $\text{MnO}_2$  and UV, which accelerated BPA removal beyond the sum of the rates achieved by the independent  $\text{MnO}_2/\text{PS}$  and  $\text{UV}/\text{PS}$

processes. To explore the mechanism of the MnO<sub>2</sub>/UV/PS process, quenching experiments were conducted as discussed in the following section.

$$\%S = \frac{k_{\text{MnO}_2/\text{UV/PS}} - (k_{\text{MnO}_2/\text{PS}} + k_{\text{UV/PS}})}{k_{\text{MnO}_2/\text{UV/PS}}} \times 100 \quad (1)$$

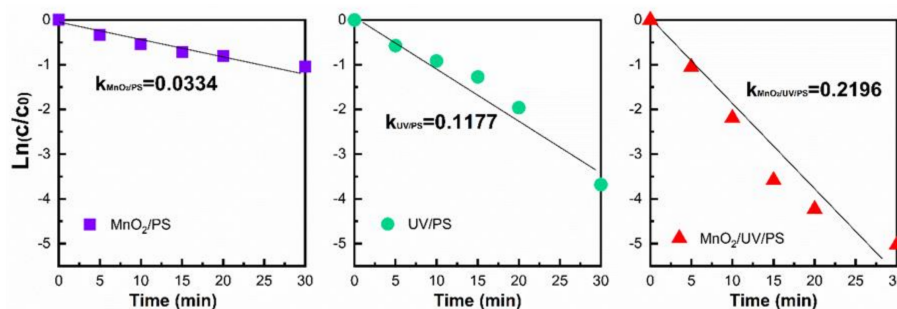
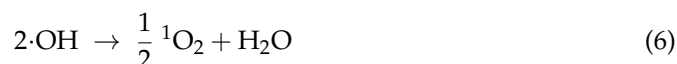
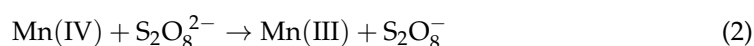


**Figure 3.** BPA degradation using MnO<sub>2</sub>/PS, UV/PS, and MnO<sub>2</sub>/UV/PS processes over 30 min. *k* = rate constant of pseudo-first-order kinetics. Conditions at *t* = 0 min: [BPA] = 30 mg/L, [PS] = 1 mM, [MnO<sub>2</sub>] = 0.25 g/L, pH = 6.5.

### 2.3.2. Contribution of ROS (•OH, SO<sub>4</sub><sup>•−</sup>, and <sup>1</sup>O<sub>2</sub>)

To elucidate the ROS involved in the MnO<sub>2</sub>/PS, UV/PS, and MnO<sub>2</sub>/UV/PS processes for BPA catalytic degradation, quenching experiments using MeOH, TBA, and FFA were carried out. The UV/MnO<sub>2</sub> process was also tested as a control. The MeOH could rapidly react with both SO<sub>4</sub><sup>•−</sup> (*k* = 2.5 × 10<sup>7</sup> M<sup>−1</sup>s<sup>−1</sup>) and •OH (*k* = 9.7 × 10<sup>8</sup> M<sup>−1</sup>s<sup>−1</sup>), and TBA could rapidly quench •OH with a rate constant in the range of 3.8–7.6 × 10<sup>8</sup> M<sup>−1</sup>s<sup>−1</sup> [25]. As the rate constant for TBA quenching of •OH was 1000 times higher than that with SO<sub>4</sub><sup>•−</sup>, it was frequently employed as a •OH scavenger [28]. The FFA was confirmed to effectively quench singlet oxygen (<sup>1</sup>O<sub>2</sub>) with a rate constant of 1.2 × 10<sup>8</sup> M<sup>−1</sup>s<sup>−1</sup> [35,36]. Therefore, in this study, MeOH (1 M), TBA (1 M), and FFA (5 mM) were used to distinguish between SO<sub>4</sub><sup>•−</sup>, •OH, and <sup>1</sup>O<sub>2</sub>, respectively. All the scavenger concentrations were excessive according to previous studies [37]. The dynamic performance of the above four BPA catalytic degradation processes was evaluated in the same conditions.

The control test showed that only limited <sup>1</sup>O<sub>2</sub> and •OH could be generated in the UV/MnO<sub>2</sub> process to degrade BPA (Figure S2). In the MnO<sub>2</sub>/PS process (Figure 4a), FFA slightly inhibited BPA degradation by decreasing BPA removal efficiency from 65.0% to 62.0%, while a 55.0% removal rate was observed with TBA; however, MeOH showed the strongest inhibition effect by decreasing the BPA removal efficiency to 40.0%, indicating that SO<sub>4</sub><sup>•−</sup> had a significant contribution in the MnO<sub>2</sub>/PS process. Several chemical reactions likely occurred, resulting in the generation of ROS. Initially, the SO<sub>4</sub><sup>•−</sup> species could be generated according to Equations (2) and (3) [38]. Subsequently, more radicals were produced by the chain reactions initiated by SO<sub>4</sub><sup>•−</sup>, producing •OH and <sup>1</sup>O<sub>2</sub> species (Equations (4)–(6)) [37,39]. The quenching experiments proved that the ROS would attack and degrade BPA (Equation (7)).



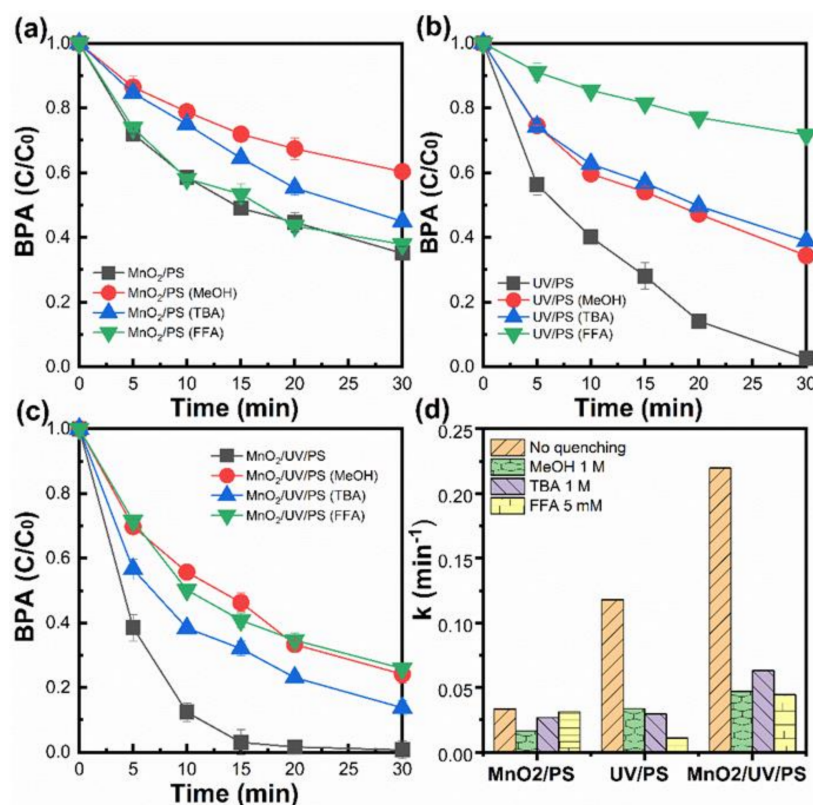


**Figure 4.** Effects of radical inhibitors on BPA concentrations over 30 min for (a) MnO<sub>2</sub>/PS, (b) UV/PS, and (c) MnO<sub>2</sub>/UV/PS processes, and (d) the effects these inhibitors have on the process rate constants. Initial conditions: [BPA] = 30 mg/L, pH = 6.5, [PS] = 1 mM, [MnO<sub>2</sub>] = 0.25 g/L. When an inhibitor is used, initial [MeOH] = 1 M or [TBA] = 1 M or [FFA] = 5 mM.

As shown in Figure 4b, the removal efficiency of BPA in the UV/PS process decreased from 97.0% to 66.0%, 61.0%, and 28.0% after MeOH, TBA, and FFA were added, respectively. These results indicate that SO<sub>4</sub><sup>•−</sup>, •OH, and <sup>1</sup>O<sub>2</sub> were generated, and the <sup>1</sup>O<sub>2</sub> species played a crucial role, followed by SO<sub>4</sub><sup>•−</sup> and •OH. Unlike in the MnO<sub>2</sub>/PS process, upon irradiation with UV light, the peroxy acid O–O bond reportedly underwent a cleavage reaction and generated two equivalents of SO<sub>4</sub><sup>•−</sup> (Equation (7)) [40]. Consequently, ROS such as •OH and <sup>1</sup>O<sub>2</sub> were converted through Equations (4) and (6) [37,39] and further reacted with BPA. Wang et al. [41] confirmed that <sup>1</sup>O<sub>2</sub> was generated under UV irradiation but that this reaction had little effect on the mineralization of organic species. Our study confirmed that the UV/PS process achieved a high BPA removal rate, albeit a lower TOC removal rate (Figure 1b), in agreement with Wang, Teng, Hu, Wu, Huang, Luo, and Christie [41].



The BPA removal efficiency of the MnO<sub>2</sub>/UV/PS process decreased from 100.0% to 76.0%, 86.0%, and 74.0% in the presence of MeOH, TBA, and FFA, respectively (Figure 4c). These findings indicate that plenty of SO<sub>4</sub><sup>•−</sup>, •OH, and <sup>1</sup>O<sub>2</sub> species were generated to decompose BPA (Figure 4d). Among these ROS, <sup>1</sup>O<sub>2</sub> and SO<sub>4</sub><sup>•−</sup> played more critical roles than •OH. The above reactions (Equations (2)–(8)) may also occur in the synergistic process. Given that <sup>1</sup>O<sub>2</sub> had little effect on the mineralization rate of organics, more robust degradation and mineralization occurred when SO<sub>4</sub><sup>•−</sup> attacked the BPA. The detailed parameters before and after quenching experiments are displayed in Table S1. To better understand the interaction between UV irradiation and MnO<sub>2</sub>, more characterization analyses of MnO<sub>2</sub> are discussed below.

#### 2.4. Infrared Spectra of MnO<sub>2</sub> and Mn Leaching in Different Processes

The ATR-FTIR spectra of the MnO<sub>2</sub> particles (Figure 5a) contained several distinct peaks with different changes after 2 h of treatment with the MnO<sub>2</sub>, UV/MnO<sub>2</sub>, MnO<sub>2</sub>/PS, and MnO<sub>2</sub>/UV/PS processes. The bands at around 720 and 650 cm<sup>-1</sup> were assigned to the Mn–O stretching and bending vibrations within a MnO<sub>6</sub> octahedral coordination environment [42,43]. The interactions between manganese and other factors (e.g., UV, persulfate, and BPA) were revealed in the range of 2500 to 1000 cm<sup>-1</sup> [42]. The band at around 1120 cm<sup>-1</sup> could be assigned to vibrations of Mn–OH bonds [44]. A blue-shift of about 52 cm<sup>-1</sup> was observed in both UV/MnO<sub>2</sub> and MnO<sub>2</sub>/UV/PS processes, indicating UV irradiation could affect the bond between Mn and OH. Two bands at around 1653 and 1546 cm<sup>-1</sup> represented the vibrations related to the interactions between Mn centers with OH and related surface groups [45]. A blue shift of about 48 cm<sup>-1</sup> at the peak position 1546 cm<sup>-1</sup> was observed in the MnO<sub>2</sub>/PS and MnO<sub>2</sub>/UV/PS processes, which suggests that PS might affect the MnO<sub>2</sub> surface. A new peak appeared at around 3380 cm<sup>-1</sup>, which only occurred in the MnO<sub>2</sub>/UV/PS process, attributing to the single bond –OH stretching vibration on the MnO<sub>2</sub> surface. For heterogeneous catalytic reactions, the degradation of organics mostly occurred on the surface of the catalyst. The –OH groups on the surface of metal oxides would enhance peroxide activation since they could make a bridge between peroxides and metal oxide surfaces [46,47]. Therefore, the generated –OH groups on the MnO<sub>2</sub> surface might improve BPA degradation in MnO<sub>2</sub>/UV/PS process.

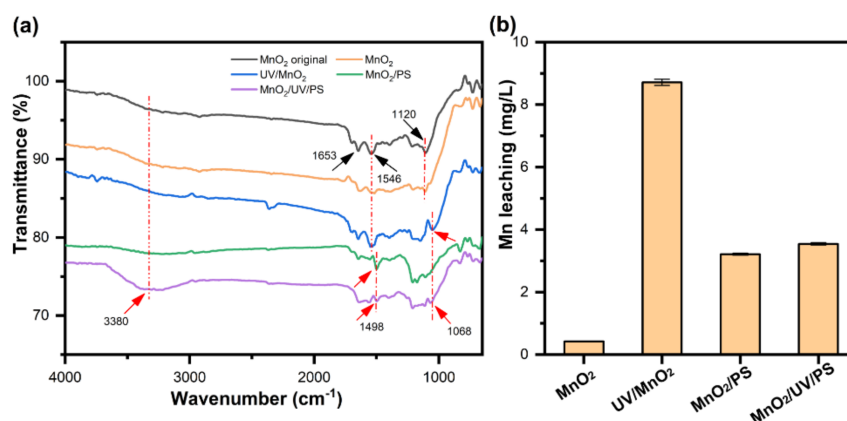


**Figure 5.** ATR-FTIR spectra of MnO<sub>2</sub> particles (a) and the concentration of Mn leaching (b) after 2 h treatment via MnO<sub>2</sub> only, UV/MnO<sub>2</sub>, MnO<sub>2</sub>/PS, and MnO<sub>2</sub>/UV/PS processes.

The ICP-OES was further applied to identify Mn leaching after 2 h of treatment in MnO<sub>2</sub>, UV/MnO<sub>2</sub>, MnO<sub>2</sub>/PS, and MnO<sub>2</sub>/UV/PS processes (Figure 5b). Limited Mn leaching in the MnO<sub>2</sub> process indicates that only a small amount of MnO<sub>2</sub> might be involved in BPA oxidation, which is consistent with the results of the BPA degradation experiments (Figure 1). In contrast, in the UV/MnO<sub>2</sub> process, the Mn leaching was significantly increased to 8.71 mg/L. Therefore, UV irradiation could stimulate the surface of MnO<sub>2</sub> to produce more Mn ions. The Mn leaching (3.21 mg/L) was relatively moderate in the MnO<sub>2</sub>/PS process. Intriguingly, compared with the MnO<sub>2</sub>/PS process, only 0.30 mg/L of Mn leaching was increased in the MnO<sub>2</sub>/UV/PS process. In the UV/MnO<sub>2</sub> process, high Mn leaching had little effect on BPA mineralization (Figure 1b). Fortunately, in the UV/MnO<sub>2</sub>/PS process, Mn leaching was greatly reduced, and BPA mineralization was significantly increased. When PS was present, UV irradiation might promote the formation of –OH groups on the surface of MnO<sub>2</sub> to protect the structure of MnO<sub>2</sub> and decrease Mn leaching.

A relatively high concentration of Mn leaching was observed in our study, mainly due to the long reaction time (2 h) for organic mineralization (e.g., over 90.0% TOC removed). Relatively low concentrations of Mn leaching were reported given the short reaction time (less than 1 h), in which thorough mineralization of organics was not consid-

ered [28,47,48]. In future research, we aim to investigate methods to decrease Mn leaching while maintaining high organic mineralization.

### 2.5. Reusability of $MnO_2$

To test the reusability of the photocatalyst,  $MnO_2$  particles were recovered and reused five times with the same initial conditions in the  $MnO_2/PS$  and  $MnO_2/UV/PS$  processes. As shown in Figure 6, the removal rate of BPA in the  $MnO_2/UV/PS$  process was 100.0% in the first three recycles and only decreased by 12.0% after five recycles; however, the removal rate of BPA continuously decreased from the initial 65.0% to 34.0% in the  $MnO_2/PS$  process. The  $MnO_2$  particles in the  $MnO_2/UV/PS$  process showed excellent stability for BPA degradation; this may be because the surface hydroxyl groups were generated under UV irradiation, which was confirmed by the ATR-FTIR results (Figure 5a). The recovered  $MnO_2$  particles had obvious agglomeration from the fourth cycle, leading to decreased surface contact with PS and reduced BPA removal. In addition, both XRD (Figure S3) and SEM (Figure S4) results manifested no significant change of the crystal structure, and morphology of  $MnO_2$  was observed after reactions in the  $MnO_2/UV/PS$  process.

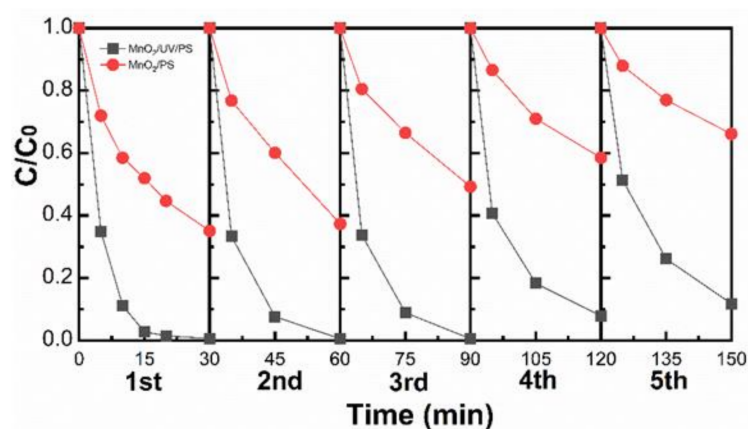


Figure 6.  $MnO_2$  recycles in  $MnO_2/PS$  and  $MnO_2/UV/PS$  processes.

### 2.6. Proposed Degradation Products and Pathways

To determine the BPA catalytic degradation pathways and intermediates under the  $MnO_2/UV/PS$  process, the reaction solutions (after 5, 15, 30, 60, 90, and 120 min) were subjected to a GC-MS analysis after extraction and derivatization. As shown in Table S2, 13 products were identified as their silylated derivatives, some of which had been proposed in previous studies. The fragment ions for both BPA and intermediates are given in Figure S5. Some degradation products may have remained unidentified in this study, as not all components could be effectively extracted into methylene chloride.

Based on the intermediates identified by GC-MS, BPA catalytic degradation via the  $MnO_2/UV/PS$  process, we propose that they occur in five steps (Figure 7). Both charge and spin densities, calculated using density functional theory, indicate that the 1, 2, 4, 6, and 7 positions of BPA (shown in red in Figure 7 top) were the most susceptible to free radical attacks [30,49]. In the first step, attacks at positions 2 and 6 were considered, and the BPA oxidative condensation through C–C and ether bridges between two phenyl rings led to the formation of dimers, such as P12 and P13. Previous studies confirmed that such condensation reactions commonly occurred upon the oxidation of phenolic compounds [50,51]. It is worth noting that these dimers were very unstable and gradually decomposed as the reaction proceeded (Figure S6). In the second step, it was presumed that the free radicals attacked both BPA and the dimers formed in the first step at positions 1, 4, and 7. The rupture of phenolic C–O and O–H bonds and the C–C bond (between phenyl and isopropyl groups) led to the formation of three active species containing phenol moieties of BPA, labeled BPA-1, BPA-2, and BPA-3. In the third step, we propose that a variety of rearrangement reactions occurred among these active species. For instance,

the coupling reaction between BPA-1 and BPA-2 would generate P11. The BPA-2 was further oxidized, subsequently recombining with another molecule of BPA directly at the position of 2 to create the ether P10. The generation of P8 was formed by hydroxylation that occurred when water molecules attacked the aromatic ring through electrophilic action [52]. Meanwhile, multiple BPA intermediates were considered to undergo coupling and deprotonation reactions to generate P9. In the fourth step, the carbocation of BPA-3 could trigger a suite of oxidation, substitution, or elimination reactions to yield P1, P2, P3, P4, and P5. In detail, the BPA-3 was subject to deprotonation to give P4 or substitution by hydroxyl, yielding P2. The elimination reaction of P2 produced P3. The BPA-3 could be subject to ketonization, generating P5, or elimination reaction, producing P1. Subsequently, the fifth step would take place with the cleavage of the phenyl rings by a free radical attack. Long-chain carboxylic acids would be produced during this step by the combination of fragments (P6 and P7) [51,53]. Finally, these long-chain compounds would continue to be converted into small molecules, such as oxalic and malonic acids [54], and ultimately into carbon dioxide and water.

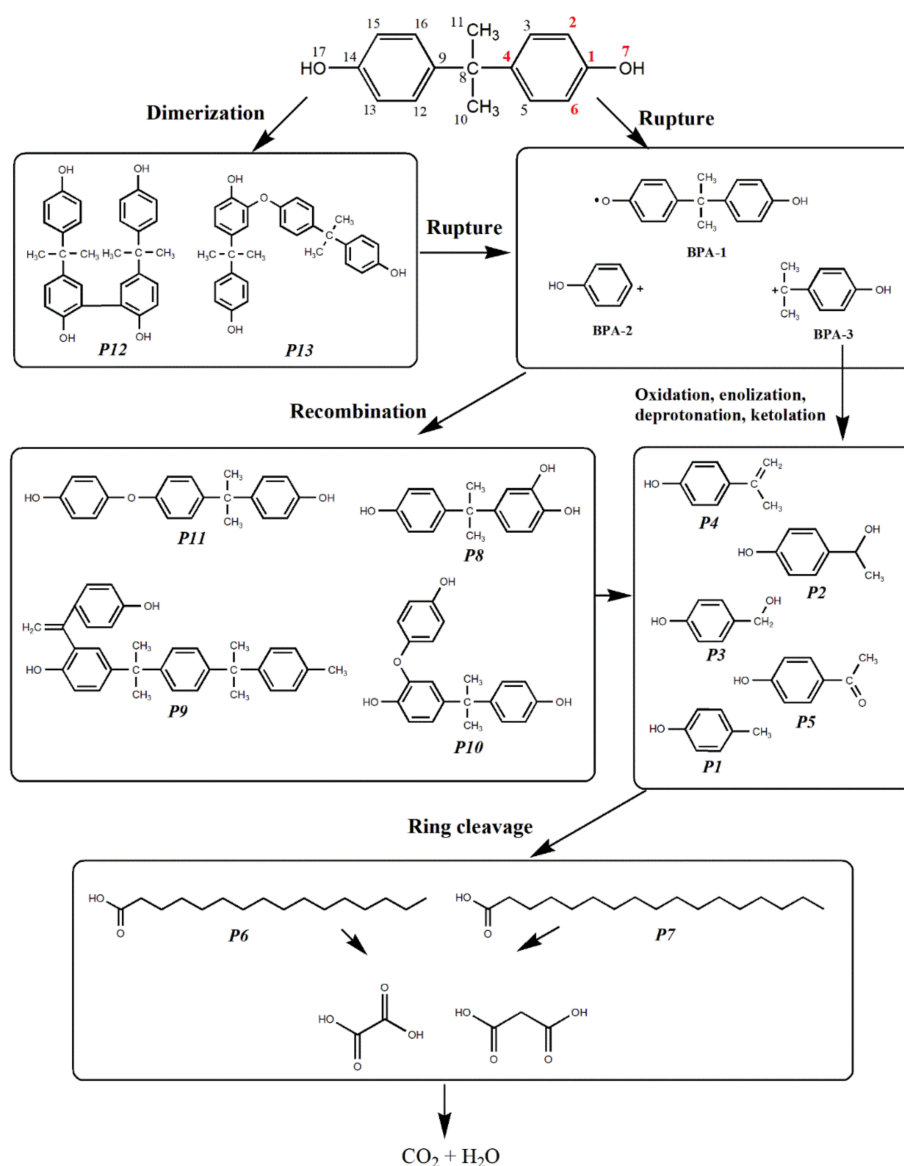


**Figure 7.** Proposed main BPA degradation pathways with steps leading to the intermediates identified using GC-MS (Table S2) under the MnO<sub>2</sub>/UV/PS process.

### 2.7. Acute Toxicity Evaluation

The toxicity of the BPA solution in the  $\text{MnO}_2/\text{UV}/\text{PS}$  process was monitored over 2 h with and without a buffer (pH 6.5). The estimated  $\text{EC}_{50}$  value of the initial BPA solution was 2.06 mg/L in the present study, which is lower than previous reports (3.46–7.7 mg/L) [55,56]; this may be because the  $\text{MnO}_2$  and PS were present in our initial BPA sample, causing the increased toxicity. Given these influencing factors, we evaluated a relative trend of the toxicity changes in the reaction process. Moreover, the samples were diluted four-fold before testing to concentrations that help provide a consistent instrumental response.

As shown in Figure 8, the  $\text{EC}_{50}$  value increased from 17.5% to 75.0% within 30 min, and then gradually decreased to 27.7% after 2 h without buffer. In the unbuffered process, the pH decreased from 6.5 for the initial BPA solution to 5.5 after 30 min, and to 2.9 after 120 min. Considering that luminescent bacterial metabolism is inhibited by overly acidic environments, as the pH value of the reaction mixture decreased, the increase in toxicity was observed by declining bioluminescence. In order to discern the effect of pH on the toxicity determination, a phosphate buffer was used to maintain the pH of the reaction mixture at 6.5. We observed that the  $\text{EC}_{50}$  value decreased slightly by 3.3% after the first 30 min of the process, followed by a substantial four-fold increase by 82.5% after 2 h. In the above discussion and Figure 1, we confirmed that the concentration of BPA and TOC of the reaction mixture decreased rapidly, especially in the first 30 min; therefore, we conclude that the increased toxicity observed in the first 30 min could be caused by some BPA degradation intermediates. Figure S6 shows that the intermediates were observed after the first 30 min of the process and that most of these gradually degraded at process times of between 30 and 120 min. These results are consistent with the toxicity test.

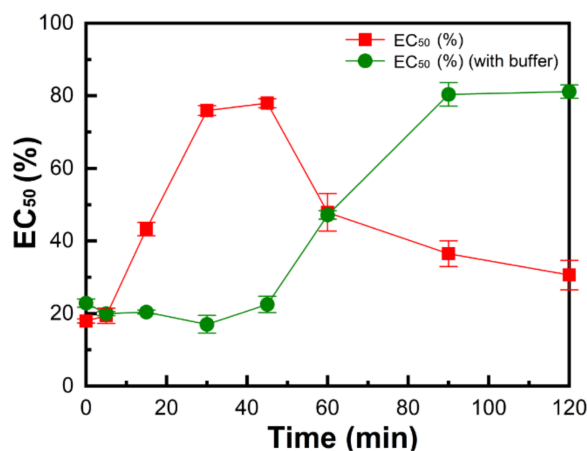


**Figure 8.**  $\text{EC}_{50}$  of  $\text{MnO}_2/\text{UV}/\text{PS}$  process mixtures determined after four-fold dilution with the Microtox<sup>®</sup> Basic test. Initial conditions: [BPA] = 30 mg/L, [PS] = 1 mM, [ $\text{MnO}_2$ ] = 0.25 g/L, with (out) phosphate buffer, pH = 6.5.

## 3. Materials and Methods

### 3.1. Chemicals and Reagents

BPA (2, 2-bis (4-hydroxyphenyl) propane, purity > 99%),  $\text{MnO}_2$  (particle size = 10  $\mu\text{m}$ ), sodium persulfate (PS, purity > 99%), methanol (MeOH), tert-butyl alcohol (TBA), furfuryl alcohol (FFA), sodium acetate, acetic acid, sodium monohydrogen phosphate, disodium hydrogen phosphate, sodium carbonate, bicarbonate, toluene, and phosphoric acid were purchased from Sigma-Aldrich (Oakville, ON, Canada). N, O-bis(trimethylsilyl)trifluoroacetamide with trimethylchlorosilane (BSTFA + TMCS) for gas chromatography derivatization, LiChropur<sup>™</sup>, containing 1% TMCS, 99% (excluding TMCS) was purchased from Sigma-Aldrich (Oakville, ON, Canada), as well.

### 3.2. Degradation Experiments

All degradation experiments were conducted in 200 mL glass bottles placed on a room temperature shaker (280 r/min) (Figure S7). A 30 mg/L sample of the BPA solution prepared with deionized water was placed in each glass bottle. PS (1 mM) and MnO<sub>2</sub> (0.25 g/L) were added into each glass bottle. A UV-254 nm (UVP 90-0012-01 Model) source (Krackeler Scientific, Albany, NY, USA) was used to treat the solutions. The UV lamp was inserted into the glass bottle and protected by a quartz tube. The tinfoil was wrapped outside the glass bottle to ensure that the experiment was carried out safely (Figure S7). In the evaluation of the impact of solution pH, different buffers were adopted using sodium acetate and acetic acid for pH 3.6 and 5.0, sodium dihydrogen phosphate and disodium hydrogen phosphate for pH 6.5 and 8.0, and sodium carbonate and bicarbonate for pH 10.0.

### 3.3. Analysis of Water Samples

The water samples were collected by syringe and first filtered through 0.22 µm membrane filters, and the BPA concentrations were analyzed using a high-performance liquid chromatography (HPLC) instrument with a C18 column (Agilent 1260 Infinity II, Mississauga, ON, Canada). An acetonitrile/water (50:50, v/v) mixture was used as a mixed mobile phase at a flow rate of 1 mL/min. The detection wavelength was 276 nm. Under these conditions, the BPA peak in the chromatogram corresponds to an elution time of 6.24 min. The total organic carbon (TOC) concentrations were measured by the burning oxidation-non-dispersive infrared absorption method using a Shimadzu TOC-L analyzer (Shimadzu, Tokyo, Japan). Phosphoric acid was added into the samples before measuring TOC to maintain the solution pH < 1. The pH was measured using a pH meter (EL20, Mettler Toledo®, Mississauga, ON, Canada). The PS concentrations were detected following a modified spectrophotometric method [57] (Text S1). The leached Mn concentrations in different processes were measured using an inductively coupled plasma optical emission spectrometer (ICP-OES, LabX, Midland, ON, Canada).

### 3.4. Characterization and Recovery of MnO<sub>2</sub>

The surface functional groups of MnO<sub>2</sub> before and after degradation reaction in MnO<sub>2</sub>, UV/MnO<sub>2</sub>, MnO<sub>2</sub>/PS, and MnO<sub>2</sub>/UV/PS processes were characterized using Fourier-transform infrared spectroscopy with attenuated total reflectance (ATR-FTIR). Other characterization methods (XRD and SEM) are listed in the supplementary materials (Text S2). Based on the XRD results, the MnO<sub>2</sub> used in this study is consistent with the phase of β-MnO<sub>2</sub>; this phase had the highest efficiency on PS activation [37]. MnO<sub>2</sub> particles were recovered and dried in a vacuum oven (Fisherbrand Isotemp Model 281A, Fisher Scientific, Ottawa, ON, Canada, set at 60 °C, 12 h).

### 3.5. Intermediates Analysis

To analyze the BPA degradation intermediates in the MnO<sub>2</sub>/UV/PS process, the reaction solutions (at 0, 5, 15, 30, 60, 90, and 120 min) were analyzed using Agilent 7890 GC coupled with an Agilent 5975 MS (Agilent technologies, Mississauga, ON, Canada). The details of BPA extraction, derivatization, and GC-MS analysis methods were based on previous studies [30,58,59] (Text S3).

### 3.6. Toxicity Evaluation

Acute toxicity tests of the MnO<sub>2</sub>/UV/PS-treated samples were carried out using a Microtox® Model 500 (M500) analyzer, whose primary indicator is the luminous bacterium *Vibrio fischeri*. The acute toxicity test relies on bacterial luminescence via cellular respiration. Inhibition of cellular activity (caused by exposure to toxins, acidic or alkaline conditions, etc.) decreases the respiratory rate, leading to a corresponding decrease in luminosity. The pH range of 6.0–8.5 is recommended to be the standard since *V. fisheryi* is pH-sensitive [60]. The toxicity testing of BPA and its intermediates were conducted both with and without phosphate buffer (pH = 6.5). In addition to BPA, the presence

of MnO<sub>2</sub> particles, PS, etc., would affect the light-emitting bacteria, so each sample was diluted before testing. To ensure consistency, the first sample was quickly obtained in the presence of MnO<sub>2</sub> and PS. Therefore, the measured effective concentration that was given the half-maximal response (EC<sub>50</sub>) of the original BPA might differ from the value given in the literature [55,56].

#### 4. Conclusions

This study proposed an integrated MnO<sub>2</sub>/UV-activated PS process for BPA catalytic degradation and demonstrated that the synergistic use of MnO<sub>2</sub> and UV is a more powerful hybrid catalyst of PS in this AOP. The mineralization of the MnO<sub>2</sub>/UV/PS process was significantly improved in comparison with MnO<sub>2</sub> or UV as a single catalyst. This process also showed a stable removal efficiency with a large variation of pH levels (3.6 to 10.0). The presence of SO<sub>4</sub><sup>•−</sup> and <sup>1</sup>O<sub>2</sub> was the key to the more rapid decomposition of BPA. Infrared spectra showed that UV irradiation could stimulate the generation of –OH groups on the MnO<sub>2</sub> surface, facilitating the PS activation in this process. The degradation pathways consisting of 5 steps and 13 intermediates were further investigated using GC-MS. The acute toxicity of reaction mixtures during the process was evaluated, which confirmed the overall reduction by the proposed method. These findings indicated that the combination of MnO<sub>2</sub> with UV improved PS catalytic activation as a more promising means of treating persistent and emerging organic pollutants. Our current research includes controlling the Mn leaching and applying other water matrixes (like real wastewater) to evaluate the feasibility of this process.

**Supplementary Materials:** The supplementary data, figures, and tables are provided in Supplementary Materials. The following are available online at <https://www.mdpi.com/article/10.3390/catal11040502/s1>.

**Author Contributions:** Conceptualization, G.D. and B.C.; methodology, G.D. and B.L.; resources, G.D., Y.C. and M.Y.; writing—original draft preparation, G.D.; writing—review and editing, G.D., B.L., S.R.S. and B.C.; supervision, B.C., S.R.S. and B.Z.; project administration, B.C. All authors have read and agreed to the published version of the manuscript.

**Funding:** This research received no external funding.

**Data Availability Statement:** The raw data supporting the conclusions of this article will be made available by the authors, without undue reservation, to any qualified researcher.

**Acknowledgments:** This research was supported by the Natural Sciences and Engineering Research Council of Canada (NSERC) and the Canada Foundation for Innovation (CFI), as well as the NSERC Collaborative Research and Training Experience (CREATE) Program and PEOPLE Network. S.R.S. acknowledged the support of the Government of Canada's Program of Energy Research and Development (PERD). The authors acknowledge Lindsay J. Hounjet, Natural Resources Canada, and CanmetENRGY Devon, for their valuable comments.

**Conflicts of Interest:** The authors declare no conflict of interest.

**Copyright Statement:** © Her Majesty the Queen in Right of Canada, as represented by the Minister of Natural Resources Canada, 2021.

#### References

1. Ouada, S.B.; Ali, R.B.; Leboulanger, C.; Ouada, H.B.; Sayadi, S. Effect of Bisphenol A on the extremophilic microalgal strain *Picocystis* sp. (Chlorophyta) and its high BPA removal ability. *Ecotoxicol. Environ. Saf.* **2018**, *158*, 1–8. [CrossRef] [PubMed]
2. Santangeli, S.; Maradonna, F.; Gioacchini, G.; Cobellis, G.; Piccinetti, C.C.; Dalla Valle, L.; Carnevali, O. BPA-induced deregulation of epigenetic patterns: Effects on female zebrafish reproduction. *Sci. Rep.* **2016**, *6*, 1–11. [CrossRef] [PubMed]
3. Newbold, R.R.; Jefferson, W.N.; Padilla-Banks, E. Long-term adverse effects of neonatal exposure to bisphenol A on the murine female reproductive tract. *Reprod. Toxicol.* **2007**, *24*, 253–258. [CrossRef] [PubMed]
4. Monje, L.; Varayoud, J.; Muñoz-de-Toro, M.; Luque, E.H.; Ramos, J.G. Exposure of neonatal female rats to bisphenol A disrupts hypothalamic LHRH pre-mRNA processing and estrogen receptor alpha expression in nuclei controlling estrous cyclicity. *Reprod. Toxicol.* **2010**, *30*, 625–634. [CrossRef] [PubMed]

5. Huang, Y.; Wong, C.; Zheng, J.; Bouwman, H.; Barra, R.; Wahlström, B.; Neretin, L.; Wong, M.H. Bisphenol A (BPA) in China: A review of sources, environmental levels, and potential human health impacts. *Environ. Int.* **2012**, *42*, 91–99. [[CrossRef](#)]
6. Kwak, J.I.; Moon, J.; Kim, D.; Cui, R.; An, Y.-J. Determination of the soil hazardous concentrations of bisphenol A using the species sensitivity approach. *J. Hazard. Mater.* **2018**, *344*, 390–397. [[CrossRef](#)]
7. Yamamoto, T.; Yasuhara, A.; Shiraishi, H.; Nakasugi, O. Bisphenol A in hazardous waste landfill leachates. *Chemosphere* **2001**, *42*, 415–418. [[CrossRef](#)]
8. Schwarzbauer, J.; Heim, S.; Brinker, S.; Littke, R. Occurrence and alteration of organic contaminants in seepage and leakage water from a waste deposit landfill. *Water Res.* **2002**, *36*, 2275–2287. [[CrossRef](#)]
9. Xiao, C.; Wang, L.; Zhou, Q.; Huang, X. Hazards of bisphenol A (BPA) exposure: A systematic review of plant toxicology studies. *J. Hazard. Mater.* **2020**, *384*, 121488. [[CrossRef](#)]
10. Haffner, D.; Schecter, A. Persistent organic pollutants (POPs): A primer for practicing clinicians. *Curr. Environ. Health Rep.* **2014**, *1*, 123–131. [[CrossRef](#)]
11. McBean, E. Removal of emerging contaminants: The next water revolution. *J. Environ. Inform. Lett.* **2019**, *1*, 1–7. [[CrossRef](#)]
12. Cao, Y.; Yu, M.; Dong, G.; Chen, B.; Zhang, B. Digital PCR as an emerging tool for monitoring of microbial biodegradation. *Molecules* **2020**, *25*, 706. [[CrossRef](#)] [[PubMed](#)]
13. Ghernaout, D.; Elboughdiri, N. Advanced oxidation processes for wastewater treatment: Facts and future trends. *Open Access Libr. J.* **2020**, *7*, 1–15. [[CrossRef](#)]
14. Liu, B.; Chen, B.; Zhang, B.; Song, X.; Zeng, G.; Lee, K. Photocatalytic ozonation of offshore produced water by TiO<sub>2</sub> nanotube arrays coupled with UV-LED irradiation. *J. Hazard. Mater.* **2021**, *402*, 123456. [[CrossRef](#)] [[PubMed](#)]
15. Oh, W.-D.; Dong, Z.; Lim, T.-T. Generation of sulfate radical through heterogeneous catalysis for organic contaminants removal: Current development, challenges and prospects. *Appl. Catal. B Environ.* **2016**, *194*, 169–201. [[CrossRef](#)]
16. Lin, Y.-T.; Chiu, Y.-T.; Ciou, C.; Liang, C. Natural organic activator quercetin for persulfate oxidative degradation of halogenated hydrocarbons. *Environ. Sci. Water Res. Technol.* **2019**, *5*, 1064–1071. [[CrossRef](#)]
17. Zhao, Q.; Mao, Q.; Zhou, Y.; Wei, J.; Liu, X.; Yang, J.; Luo, L.; Zhang, J.; Chen, H.; Chen, H. Metal-free carbon materials-catalyzed sulfate radical-based advanced oxidation processes: A review on heterogeneous catalysts and applications. *Chemosphere* **2017**, *189*, 224–238. [[CrossRef](#)] [[PubMed](#)]
18. Li, R.; Hu, H.; Ma, Y.; Liu, X.; Zhang, L.; Zhou, S.; Deng, B.; Lin, H.; Zhang, H. Persulfate enhanced photocatalytic degradation of bisphenol A over wasted batteries-derived ZnFe<sub>2</sub>O<sub>4</sub> under visible light. *J. Clean. Prod.* **2020**, *276*, 124246. [[CrossRef](#)]
19. Wang, J.; Wang, S. Activation of persulfate (PS) and peroxymonosulfate (PMS) and application for the degradation of emerging contaminants. *Chem. Eng. J.* **2018**, *334*, 1502–1517. [[CrossRef](#)]
20. Petala, A.; Arvaniti, O.S.; Christofili, M.; Safakas, A.; Frontistis, Z.; Mantzavinos, D. Lanthanum Nickel Oxide: An Effective Heterogeneous Activator of Sodium Persulfate for Antibiotics Elimination. *Catalysts* **2020**, *10*, 1373. [[CrossRef](#)]
21. Pan, Y.; Zhang, Y.; Zhou, M.; Cai, J.; Tian, Y. Enhanced removal of emerging contaminants using persulfate activated by UV and pre-magnetized FeO. *Chem. Eng. J.* **2019**, *361*, 908–918. [[CrossRef](#)]
22. Wang, B.; Fu, T.; An, B.; Liu, Y. UV light-assisted persulfate activation by CuO-Cu<sub>2</sub>O for the degradation of sulfamerazine. *Sep. Purif. Technol.* **2020**, *251*, 117321. [[CrossRef](#)]
23. Pan, X.; Yan, L.; Li, C.; Qu, R.; Wang, Z. Degradation of UV-filter benzophenone-3 in aqueous solution using persulfate catalyzed by cobalt ferrite. *Chem. Eng. J.* **2017**, *326*, 1197–1209. [[CrossRef](#)]
24. Dong, G.; Huang, L.; Wu, X.; Wang, C.; Liu, Y.; Liu, G.; Wang, L.; Liu, X.; Xia, H. Effect and mechanism analysis of MnO<sub>2</sub> on permeable reactive barrier (PRB) system for the removal of tetracycline. *Chemosphere* **2018**, *193*, 702–710. [[CrossRef](#)]
25. Huang, J.; Dai, Y.; Singewald, K.; Liu, C.-C.; Saxena, S.; Zhang, H. Effects of MnO<sub>2</sub> of different structures on activation of peroxymonosulfate for bisphenol A degradation under acidic conditions. *Chem. Eng. J.* **2019**, *370*, 906–915. [[CrossRef](#)]
26. Mazloomi, S.; Nasser, S.; Nabizadeh, R.; Yaghmaeian, K.; Alimohammadi, K.; Nazmara, S.; Mahvi, A.H. Remediation of fuel oil contaminated soils by activated persulfate in the presence of MnO<sub>2</sub>. *Soil Water Res.* **2016**, *11*, 131–138. [[CrossRef](#)]
27. Chiam, S.-L.; Pung, S.-Y.; Yeoh, F.-Y. Recent developments in MnO<sub>2</sub>-based photocatalysts for organic dye removal: A review. *Environ. Sci. Pollut. Res.* **2020**, *27*, 5759–5778. [[CrossRef](#)]
28. Eslami, A.; Hashemi, M.; Ghanbari, F. Degradation of 4-chlorophenol using catalyzed peroxymonosulfate with nano-MnO<sub>2</sub>/UV irradiation: Toxicity assessment and evaluation for industrial wastewater treatment. *J. Clean. Prod.* **2018**, *195*, 1389–1397. [[CrossRef](#)]
29. Lee, J.; Von Gunten, U.; Kim, J.-H. Persulfate-based advanced oxidation: Critical assessment of opportunities and roadblocks. *Environ. Sci. Technol.* **2020**, *54*, 3064–3081. [[CrossRef](#)]
30. Lin, K.; Liu, W.; Gan, J. Oxidative removal of bisphenol A by manganese dioxide: Efficacy, products, and pathways. *Environ. Sci. Technol.* **2009**, *43*, 3860–3864. [[CrossRef](#)] [[PubMed](#)]
31. Huang, J.; Zhang, H. Mn-based catalysts for sulfate radical-based advanced oxidation processes: A review. *Environ. Int.* **2019**, *133*, 105141. [[CrossRef](#)]
32. Criquet, J.; Leitner, N.K.V. Degradation of acetic acid with sulfate radical generated by persulfate ions photolysis. *Chemosphere* **2009**, *77*, 194–200. [[CrossRef](#)]
33. Lominchar, M.; Santos, A.; De Miguel, E.; Romero, A. Remediation of aged diesel contaminated soil by alkaline activated persulfate. *Sci. Total Environ.* **2018**, *622*, 41–48. [[CrossRef](#)] [[PubMed](#)]

34. Frontistis, Z.; Daskalaki, V.M.; Hapeshi, E.; Drosou, C.; Fatta-Kassinos, D.; Xekoukoulotakis, N.P.; Mantzavinos, D. Photocatalytic (UV-A/TiO<sub>2</sub>) degradation of 17 $\alpha$ -ethynylestradiol in environmental matrices: Experimental studies and artificial neural network modeling. *J. Photochem. Photobiol. A Chem.* **2012**, *240*, 33–41. [[CrossRef](#)]
35. Zhou, Y.; Jiang, J.; Gao, Y.; Ma, J.; Pang, S.-Y.; Li, J.; Lu, X.-T.; Yuan, L.-P. Activation of peroxymonosulfate by benzoquinone: A novel nonradical oxidation process. *Environ. Sci. Technol.* **2015**, *49*, 12941–12950. [[CrossRef](#)]
36. Li, C.; Wu, J.; Peng, W.; Fang, Z.; Liu, J. Peroxymonosulfate activation for efficient sulfamethoxazole degradation by Fe<sub>3</sub>O<sub>4</sub>/ $\beta$ -FeOOH nanocomposites: Coexistence of radical and non-radical reactions. *Chem. Eng. J.* **2019**, *356*, 904–914. [[CrossRef](#)]
37. Zhu, S.; Li, X.; Kang, J.; Duan, X.; Wang, S. Persulfate activation on crystallographic manganese oxides: Mechanism of singlet oxygen evolution for nonradical selective degradation of aqueous contaminants. *Environ. Sci. Technol.* **2018**, *53*, 307–315. [[CrossRef](#)]
38. Zhao, Y.; Zhao, Y.; Zhou, R.; Mao, Y.; Tang, W.; Ren, H. Insights into the degradation of 2,4-dichlorophenol in aqueous solution by  $\alpha$ -MnO<sub>2</sub> nanowire activated persulfate: Catalytic performance and kinetic modeling. *RSC Adv.* **2016**, *6*, 35441–35448. [[CrossRef](#)]
39. Lu, X.; Shao, Y.; Gao, N.; Chen, J.; Zhang, Y.; Xiang, H.; Guo, Y. Degradation of diclofenac by UV-activated persulfate process: Kinetic studies, degradation pathways and toxicity assessments. *Ecotoxicol. Environ. Saf.* **2017**, *141*, 139–147. [[CrossRef](#)] [[PubMed](#)]
40. Liu, Y.; He, X.; Fu, Y.; Dionysiou, D.D. Kinetics and mechanism investigation on the destruction of oxytetracycline by UV-254 nm activation of persulfate. *J. Hazard. Mater.* **2016**, *305*, 229–239. [[CrossRef](#)]
41. Wang, A.; Teng, Y.; Hu, X.; Wu, L.; Huang, Y.; Luo, Y.; Christie, P. Photodegradation of diphenylarsinic acid by UV-C light: Implication for its remediation. *J. Hazard. Mater.* **2016**, *308*, 199–207. [[CrossRef](#)]
42. Ananth, M.; Pethkar, S.; Dakshinamurthi, K. Distortion of MnO<sub>6</sub> octahedra and electrochemical activity of Nstutite-based MnO<sub>2</sub> polymorphs for alkaline electrolytes—An FTIR study. *J. Power Sources* **1998**, *75*, 278–282. [[CrossRef](#)]
43. Xie, J.; Chen, L.; Zhou, W.-F.; Au, C.-T.; Yin, S.-F. Selective oxidation of p-chlorotoluene to p-chlorobenzaldehyde over metal-modified OMS-2 molecular sieves. *J. Mol. Catal. A Chem.* **2016**, *425*, 110–115. [[CrossRef](#)]
44. Liu, R.; Liu, H.; Qiang, Z.; Qu, J.; Li, G.; Wang, D. Effects of calcium ions on surface characteristics and adsorptive properties of hydrous manganese dioxide. *J. Colloid Interface Sci.* **2009**, *331*, 275–280. [[CrossRef](#)] [[PubMed](#)]
45. Khan, A.; Liao, Z.; Liu, Y.; Jawad, A.; Iftikhar, J.; Chen, Z. Synergistic degradation of phenols using peroxymonosulfate activated by CuO-Co<sub>3</sub>O<sub>4</sub>@MnO<sub>2</sub> nanocatalyst. *J. Hazard. Mater.* **2017**, *329*, 262–271. [[CrossRef](#)] [[PubMed](#)]
46. Ren, Y.; Lin, L.; Ma, J.; Yang, J.; Feng, J.; Fan, Z. Sulfate radicals induced from peroxymonosulfate by magnetic ferrosphenel MFe<sub>2</sub>O<sub>4</sub> (M= Co, Cu, Mn, and Zn) as heterogeneous catalysts in the water. *Appl. Catal. B Environ.* **2015**, *165*, 572–578. [[CrossRef](#)]
47. Dong, Z.; Zhang, Q.; Chen, B.-Y.; Hong, J. Oxidation of bisphenol A by persulfate via Fe<sub>3</sub>O<sub>4</sub>- $\alpha$ -MnO<sub>2</sub> nanoflower-like catalyst: Mechanism and efficiency. *Chem. Eng. J.* **2019**, *357*, 337–347. [[CrossRef](#)]
48. Huang, G.-X.; Wang, C.-Y.; Yang, C.-W.; Guo, P.-C.; Yu, H.-Q. Degradation of bisphenol A by peroxymonosulfate catalytically activated with Mn<sub>1.8</sub>Fe<sub>1.2</sub>O<sub>4</sub> nanospheres: Synergism between Mn and Fe. *Environ. Sci. Technol.* **2017**, *51*, 12611–12618. [[CrossRef](#)]
49. Yao, J.; Qu, R.; Wang, X.; Sharma, V.K.; Shad, A.; Dar, A.A.; Wang, Z. Visible light and fulvic acid assisted generation of Mn (III) to oxidize bisphenol A: The effect of tetrabromobisphenol A. *Water Res.* **2020**, *169*, 115273. [[CrossRef](#)]
50. Zhang, H.; Huang, C.-H. Reactivity and transformation of antibacterial N-oxides in the presence of manganese oxide. *Environ. Sci. Technol.* **2005**, *39*, 593–601. [[CrossRef](#)]
51. de Freitas, E.N.; Bubna, G.A.; Brugnari, T.; Kato, C.G.; Nolli, M.; Rauen, T.G.; Moreira, R.D.; Peralta, R.A.; Bracht, A.; de Souza, C.G. Removal of bisphenol A by laccases from *Pleurotus ostreatus* and *Pleurotus pulmonarius* and evaluation of ecotoxicity of degradation products. *Chem. Eng. J.* **2017**, *330*, 1361–1369. [[CrossRef](#)]
52. Lin, J.; Hu, Y.; Wang, L.; Liang, D.; Ruan, X.; Shao, S. M88/PS/Vis system for degradation of bisphenol A: Environmental factors, degradation pathways, and toxicity evaluation. *Chem. Eng. J.* **2020**, *382*, 122931. [[CrossRef](#)]
53. Molkenhain, M.; Olmez-Hanci, T.; Jekel, M.R.; Arslan-Alaton, I. Photo-Fenton-like treatment of BPA: Effect of UV light source and water matrix on toxicity and transformation products. *Water Res.* **2013**, *47*, 5052–5064. [[CrossRef](#)] [[PubMed](#)]
54. Kusvuran, E.; Yildirim, D. Degradation of bisphenol A by ozonation and determination of degradation intermediates by gas chromatography–mass spectrometry and liquid chromatography–mass spectrometry. *Chem. Eng. J.* **2013**, *220*, 6–14. [[CrossRef](#)]
55. Chiang, K.; Lim, T.M.; Tsen, L.; Lee, C.C. Photocatalytic degradation and mineralization of bisphenol A by TiO<sub>2</sub> and platinumized TiO<sub>2</sub>. *Appl. Catal. A Gen.* **2004**, *261*, 225–237. [[CrossRef](#)]
56. Tobajas, M.; Verdugo, V.; Polo, A.M.; Rodriguez, J.J.; Mohedano, A.F. Assessment of toxicity and biodegradability on activated sludge of priority and emerging pollutants. *Environ. Technol.* **2016**, *37*, 713–721. [[CrossRef](#)] [[PubMed](#)]
57. Lee, H.; Lee, H.-J.; Jeong, J.; Lee, J.; Park, N.-B.; Lee, C. Activation of persulfates by carbon nanotubes: Oxidation of organic compounds by nonradical mechanism. *Chem. Eng. J.* **2015**, *266*, 28–33. [[CrossRef](#)]
58. Sharma, J.; Mishra, I.; Dionysiou, D.D.; Kumar, V. Oxidative removal of Bisphenol A by UV-C/peroxymonosulfate (PMS): Kinetics, influence of co-existing chemicals and degradation pathway. *Chem. Eng. J.* **2015**, *276*, 193–204. [[CrossRef](#)]
59. Cao, Y.; Zhang, B.; Zhu, Z.; Song, X.; Cai, Q.; Chen, B.; Dong, G.; Ye, X. Microbial eco-physiological strategies for salinity-mediated crude oil biodegradation. *Sci. Total Environ.* **2020**, *727*, 138723. [[CrossRef](#)]
60. Johnson, B.T. Microtox<sup>®</sup> acute toxicity test. In *Small-Scale Freshwater Toxicity Investigations*; Springer: Berlin/Heidelberg, Germany, 2005; pp. 69–105.